Paper

Analysis of Selective-Decode and Forward Relaying Protocol over κ-μ Fading Channel Distribution

Ravi Shankar[1,2], Lokesh Bhardwaj[1], Ritesh Kumar Mishra[1]

[1] *National Institute of Technology Patna, Patna, India*
[2] *Madanapalle Institute of Technology and Science, Madanapalle, AP, India*

https://doi.org/10.26636/jtit.2020.135919

Abstract—In this work, the performance of selective-decode and forward (S-DF) relay systems over κ-μ fading channel conditions is examined in terms of probability density function (PDF), system model and cumulative distribution function (CDF) of the κ-μ distributed envelope, signal-to-noise ratio and the techniques used to generate samples that rely on κ-μ distribution. Specifically, we consider a case where the source-to-relay, relay-to-destination and source-to-destination link is subject to independent and identically distributed κ-μ fading. From the simulation results, the enhancement in the symbol error rate (SER) with a stronger line of sight (LOS) component is observed. This shows that S-DF relaying systems may perform well even in non-fading or LOS conditions. Monte Carlo simulations are conducted for various fading parameter values and the outcomes turn out to be a close match for theoretical results, which validates the derivations made.

Keywords—channel fading, channel state information, relaying protocol, selective decode and forward, symbol error rate.

1. Introduction

Fifth generation (5G) wireless communication systems will require a paradigm shift to meet the increasing demand for reliable connectivity offering high data rates, low latency, better energy efficiency, and femto cell-based relays [1]–[3]. Cooperative communication is the natural choice for 5G wireless communication systems, and is adopted in third generation partnership project (3GPP), universal mobile telecommunications service (UMTS), long term evolution (LTE)-Advanced and IEEE 802.11 standards, because the nodes of a cooperative communication network may share their resources with each other while transmitting the signal [4]–[6]. This approach is also incorporated into numerous 5G wireless applications, such as machine-to-machine (M2M), device-to-device (D2D), cognitive radio (CR), high speed terrestrial network (HSTN), and free space optical (FSO) communication [7]–[10].

Relay-assisted cooperation is the first step towards a 5G system that is expected to deliver up to 20 Gbps in downlink (DL) and 10 Gbps in uplink (UL) communications, serving as a benchmark for network operators during initial rollouts over the next few years [11]–[12]. The relay infrastructure does not require a wired network connection, thus offering a reduction in the operator's backhaul costs. Through the additional cooperative diversity inherent in such wireless systems, cooperative wireless communication significantly improves end-to-end reliability. If the direct source-to-destination (SD) channel is in a deep fade, the main advantage of the cooperative communication is that the destination node may still receive the source signal via the relay node.

Two basic relaying methods used for transmitting and receiving signals may be distinguished: analog and digital. Analog relaying is also referred to as non-regenerative, as the signals are not required to be digitized before they are sent. Amplify-and-forward (AF) is an example of the analog relaying approach. On the other hand, before transmitting the signals to their destination, a relay node uses the digital relay protocol to decode and encode signals. Consequently, digital relaying is also known as regenerative relaying. The main drawback of the AF protocol is noise amplification. The relay may transmit the erroneous signal to the destination node if the decode-and-forward (DF) relaying protocol is used. The S-DF protocol has been proposed to overcome the disadvantage of noise amplification and erroneous decoding related to AF and DF, respectively [13]–[17]. To overcome the problem of noise amplification and relay error propagation, the S-DF protocol is used in 5G wireless systems. S-DF relaying networks relay forward correctly decoded signals only. Otherwise, they remain idle. Moreover, network connectivity and data transmission rates of S-DF relaying may be further augmented by using multiple-input multiple-output (MIMO) in conjunction with space-time-block-code (STBC) [18].

In [19]–[20], the authors investigated an S-DF relaying network over the Rayleigh flat fading channel. In [19], the authors investigated pairwise error probability (PEP) performance of an S-DF relaying network over the Rayleigh flat fading channel, evaluating ideal channel conditions. In [21]–[23], the authors investigated an S-DF relaying network over Nakagami-*m* fading channel conditions. In [23], the authors investigated a dual hop (DH) S-DF

relaying network over frequency flat Nakagami-m fading channel conditions, evaluating ideal channel conditions. However, papers [19]–[23] did taken non-homogeneous fading channel conditions into consideration. The performance of wireless communication systems is significantly influenced by stochastic modeling and characterization of the fading links between the communicating nodes. Therefore, accurate stochastic modeling is very critical in the development of efficient wireless communication schemes and protocols.

In the literature, a variety of stochastic/statistical distributions have been developed to model small-scale fluctuations in the transmitted signal envelope over fading channels, such as Nakagami-m, Rayleigh and Weibull [24]–[26]. However, none of the stochastic models described capture the non-linearity of the propagation medium. κ-μ distribution is a suitable choice for LOS applications and, on the other hand, for non-LOS, η-μ fading distribution is better suited for non-LOS scenarios. In [27], the authors proposed η-μ and κ-μ non-homogeneous fading distributions for LOS and non-LOS components, respectively. In [28]–[33], the authors investigated a relaying network under κ-μ and η-μ fading channel conditions. In [34], the authors investigated the SER performance of a DF relaying network over η-μ and κ-μ fading channel conditions. The exact SER expression is derived for M-ary phase shift keying (PSK) modulated schemes. In this work, SER expressions are obtained for S-DF relaying networks and additional diversity gains are achieved due to use of MIMO in conjunction with STBC. Hence, we consider κ-μ fading distribution to be well suited for LOS applications.

The paper is organized as follows. In Section 2, SER is investigated over κ-μ fading channel conditions. The closed form SER expression is derived using a moment generating function (MGF)-based approach. In Section 3, simulation results are given and Section 4 presents the conclusions.

2. End-to-end Symbol Error Analysis

Let us consider a MIMO-STBC S-DF relaying network with a K number of relay nodes. In all the analyses associated with SER performance of S-DF relaying networks, we will assume $N_S \times N_R$ MIMO systems. N_S is the number of antennas existing at the source node and N_R is the number of antennas installed at the relay nodes. Since both source and relay nodes use the same orthogonal STBC code, we take $N_S = N_R = N$. It is presumed that the orthogonal STBC code is conveyed over T time slots. An orthogonal STBC codeword for complete STBC communication may be agreed by a matrix with dimensions $N_S \times T$. It was argued before that orthogonal STBC codewords may be managed in different aerials and then the data processed may be combined together in order to obtain effective results - an approach that is similar to maximum ratio combiner (MRC) [35]. Orthogonal STBC is designed such that the vectors representing any pair of columns taken from the source-to-r-th relay coding matrix H_{sr} are orthogonal, i.e. STBC converts the vector channel into a scalar channel. For orthogonal STBC designs, conditional SNR at the receiver may be given as an Euclidean or a Frobenius norm of the channel times the average SNR, as [4]:

$$\gamma_{sr} = \overline{\gamma}_{sr} \left\| H_{sr} \right\|_F^2 , \tag{1}$$

where γ_{sr} denotes the conditional SNR of the source-to-r-th relay fading link, $\overline{\gamma}_{sr}$ denotes the average conditional SNR of the source-to-r-th relay fading link and $\left\| H_{sr} \right\|_F^2$ denotes the Frobenius norm or L_2 norm. All elements of H_{sr} are i.i.d. κ-μ distributed random variables (RVs). The suggestion of κ-μ channel fading was given in [36] as a generalized distribution to model a non-homogeneous fading environment. As for η-μ and Nakagami-m fading channel distribution, it was observed that, for κ-μ fading channel conditions, the multipath components form clusters. Each cluster has several scattered multipath components. The delay spread of different clusters is relatively larger than the delay spread of multipath components within a cluster. Every cluster is assumed to have the same average power. Unlike in η-μ fading and like Nakagami-m fading, it is assumed that the in-phase and quadrature phase components are independent and have equal powers in κ-μ fading. However, each cluster is assumed to have some dominant components considered to be of the LOS variety. In such a model, the representation of the envelope of the fading signal is slightly different from that of Nakagami-m and/or η-μ fading. It may be given as [36]–[39]:

$$\beta^2 = \sum_{j=0}^{J} \left[(I_J + \phi_j)^2 + (\Omega_j + \alpha_j)^2 \right] , \tag{2}$$

where J is the number of clusters in the received signal, $(I_j + \phi_j)$ and $(\Omega_j + \alpha_j)$ are the in-phase and quadrature phase components, respectively, of the resultant signal of

Table 1
Modulation parameters for various modulation schemes [34]–[35]

Modulation scheme	a	b	c
Binary PSK	1	2	0
Binary frequency shift keying	1	1	0
M-ary-PSK	2	$2\sin^2\left(\frac{\pi}{M}\right)$	0
M-ary-pulse amplitude modulation	$2\frac{M-1}{M}$	$\frac{6}{M^2-1}$	0
Quadrature PSK	2	2	1
Coherent differential PSK	2	2	2
M-ary-quadrature amplitude modulation (QAM)	$4\frac{\sqrt{M}-1}{\sqrt{M}}$	$\frac{3}{M-1}$	$d\left(\frac{\sqrt{M}-1}{\sqrt{M}}\right)^2$

the j-th cluster. Both I_j and Ω_j are mutually independent and zero-mean circular-shift complex Gaussian (ZMCSCG), $E[I_j] = E[\Omega_j] = 0$ and have equal variance, i.e. $E[I_j^2] = E[\Omega_j^2] = \sigma^2$. ϕ_j and α_j denote the in-phase and quadrature components, respectively. The non-zero mean of in-phase and quadrature phase components reveals the presence of a dominant component in the clusters of the received signal. Again, as in the case of Nakagami-m and η-μ fading models, the fading amplitude may be expressed as:

$$\beta^2 = \sum_{j=0}^{J} \mathbb{C}_j^2 \tag{3}$$

$$\mathbb{C}_j^2 = (I_j + \phi_j)^2 + (\Omega_j + \alpha_j)^2 \ . \tag{4}$$

From the fact that I_j and Ω_j are Gaussian distributed, it is to be noted here that $\mathbb{C}_j^2$ follows non-central Chi-squared distribution. Unlike Nakagami-m and η-μ channel models, κ-μ distribution is suitable for model LOS environments. PDF of SNR for an STBC MIMO system over κ-μ fading channels may be given by [36]–[39]:

$$p_{\gamma_{sr}}(\gamma_{sr}) = \frac{\mu_{sr} N_S N_R (1+\kappa_{sr})^{\frac{\mu_{sr} N_S N_R + 1}{2}}}{(\kappa_{sr})^{\frac{\mu_{sr} N_S N_R - 1}{2}} \mathrm{e}^{\mu_{sr} N_S N_R \kappa_{sr}} \overline{\gamma}^{\frac{\mu_{sr} N_S N_R + 1}{2}}} \gamma_{sr}^{\frac{\mu_{sr} N_S N_R - 1}{2}} \mathrm{e}^{-\frac{\mu_{sr} N_S N_R (1+\kappa_{sr}) \gamma_{sr}}{\overline{\gamma}_{sr}}} I_{\mu_{sr} N_S N_R - 1}\left(2\mu_{sr} N_S N_R \sqrt{\frac{\kappa_{sr}(1+\kappa_{sr})\gamma_{sr}}{\overline{\gamma}_{sr}}}\right), \tag{5}$$

where $\mu_{sr} > 0$ is the channel fading parameter directly related to the number of clusters, κ_{sr} denotes the ratio of power in the LOS components to that of scattered components. Note that $\overline{\gamma}_{sr}$ is the expected SNR and is used as a scaling factor of $\|H_{sr}\|_F^2$ in existing literature to indicate average SNR at the receiver. The instantaneous SER $P_E^{S\to R}(\gamma_{sr})$ of the source-to-r-th relay fading link may be expressed as [40]–[41]:

$$P_E^{S\to R}(\gamma_{sr}) = aQ\left(\sqrt{b\gamma_{sr}}\right) - cQ^2\left(\sqrt{b\gamma_{sr}}\right) \ , \tag{6}$$

where a, b and c are modulation-dependent parameters listed in Table 1 and $Q(.)$ represents the Gaussian Q function describing the area under the tail of a Gaussian curve and is defined as [40]–[41]:

$$Q(x) = \frac{1}{\sqrt{2\pi}} \int_x^{\infty} \mathrm{e}^{-\frac{u^2}{2}} \mathrm{d}u = \frac{1}{\sqrt{\pi}} \int_x^{\infty} \mathrm{e}^{-z^2} \mathrm{d}z = \frac{\mathrm{erfc}(x)}{2} \ , \tag{7}$$

where $\mathrm{erfc}(x)$ is the complementary error function, which is accessible, inter alia, in Matlab.
The expected SER $\overline{P_E^{S\to R}}$ may be obtained by taking expectation of the instantaneous SER over the PDF of receiving instantaneous SNR. For averaging the conditional SER, we will use the MGF-based approach. It may be expressed as [40]:

$$\overline{P_E^{S\to R}} = \underbrace{\frac{a}{\pi} \int_0^{\frac{\pi}{2}} M_{\gamma_{sr}}\left(\frac{b}{2\sin^2\theta}\right) \mathrm{d}\theta}_{I_1} - \underbrace{\frac{c}{\pi} \int_0^{\frac{\pi}{4}} M_{\gamma_{sr}}\left(\frac{b}{2\sin^2\theta}\right) \mathrm{d}\theta}_{I_2} \ , \tag{8}$$

where $M_{\gamma_{sr}}(.)$ is the MGF of the received conditional SNR. MGF of κ-μ distributed instantaneous SNR is given as [40]–[41]:

$$M_{\gamma_{sr}}(s) = \int_0^{\infty} p_{\gamma_{sr}}(\gamma_{sr}) \mathrm{e}^{-s\gamma_{sr}} \mathrm{d}\gamma_{sr} = \left(\frac{\mu_{sr} N_S N_R (1+\kappa_{sr})}{\mu_{sr} N_S N_R (1+\kappa_{sr}) + s\overline{\gamma}_{sr}}\right)^{\mu_{sr} N_S N_R} \mathrm{e}^{\left(\frac{(\mu_{sr} N_S N_R)^2 \kappa_{sr}(1+\kappa_{sr})}{\mu_{sr} N_S N_R (1+\kappa_{sr}) + s\overline{\gamma}_{sr}}\right) - \kappa_{sr}\mu_{sr} N_S N_R} . \tag{9}$$

I_1 may be expressed in terms of a confluent hypergeometric function [42], as evaluated in Appendix A.

$$I_1 = \frac{a}{\pi} \frac{\sqrt{b\overline{\gamma}_{sr}} (\mu_{sr} N_S N_R \kappa_{sr})^{\mu_{sr} N_S N_R}}{\sqrt{2\pi\mu_{sr} N_S N_R (1+\kappa_{sr})}} \left(\frac{2\mu_{sr} N_S N_R (1+\kappa_{sr})}{2\mu_{sr} N_S N_R (1+\kappa_{sr}) + b\overline{\gamma}_{sr}}\right)^{\mu_{sr} N_S N_R + \frac{1}{2}} \frac{\Gamma\left(\mu_{sr} N_S N_R + \frac{1}{2}\right)\sqrt{\pi}}{\Gamma(\mu_{sr} N_S N_R + 1)} \times$$

$$\sum_{J=0}^{\infty} \sum_{n=0}^{\infty} \frac{\left(\mu_{sr} N_S N_R + \frac{1}{2}\right)_{J+n} (1)_J \left(\frac{2\mu_{sr} N_S N_R (1+\kappa_{sr})}{2\mu_{sr} N_S N_R (1+\kappa_{sr}) + b\overline{\gamma}_{sr}}\right)^J \left(\frac{2\mu_{sr} N_S N_R (1+\kappa_{sr})}{2\mu_{sr} N_S N_R (1+\kappa_{sr}) + b\overline{\gamma}_{sr}}\right)^n}{(\mu_{sr} N_S N_R + 1)_{J+n} J! n!} \ . \tag{10}$$

where $\Gamma(x)$ represents the Gamma function [42] and $(x)_n$ denotes the descending factorial [44]–[45], $(x)_n = \dfrac{\Gamma(x+1)}{\Gamma(x-n+1)}$.

I_2 may be expressed in terms of confluent Lauricella's hypergeometric function [43], as evaluated in Appendix B.

$$I_2 = \frac{c\sqrt{b\overline{\gamma}_{sr}}(\mu_{sr}N_SN_R\kappa_{sr})^{\mu_{sr}N_SN_R}}{2\pi\sqrt{2\mu_{sr}N_SN_R(1+\kappa_{sr})}}\left(\frac{\mu_{sr}N_SN_R(1+\kappa_{sr})}{\mu_{sr}N_SN_R(1+\kappa_{sr})+b\overline{\gamma}_{sr}}\right)^{\mu_{sr}N_SN_R+\frac{1}{2}}\frac{\Gamma\left(\mu_{sr}N_SN_R+\frac{1}{2}\right)\sqrt{\pi}}{\Gamma(\mu_{sr}N_SN_R+1)}\times$$

$$\sum_{J=0}^{\infty}\sum_{n=0}^{\infty}\sum_{p=0}^{\infty}\frac{\left(\mu_{sr}N_SN_R+\frac{1}{2}\right)_{J+N+P}(1)_m\left(\frac{1}{2}\right)_n\left(\frac{\mu_{sr}N_SN_R(1+\kappa_{sr})}{\mu_{sr}N_SN_R(1+\kappa_{sr}+b\overline{\gamma}_{sr}}\right)^J\left(\frac{2\mu_{sr}N_SN_R(1+\kappa_{sr})}{2\mu_{sr}N_SN_R(1+\kappa_{sr})+2b\overline{\gamma}_{sr}}\right)^n\left(\frac{\mu_{sr}N_SN_R(1+\kappa_{sr})}{\mu_{sr}N_SN_R(1+\kappa_{sr})+b\overline{\gamma}_{sr}}\right)^n}{\left(\frac{3}{2}\right)_{J+N+P}J!n!p!}. \quad (11)$$

Following a similar analysis, the SER for the S→D fading link may be given as [40]:

$$\overline{P_E^{S\to D}} = \underbrace{\frac{a}{\pi}\int_0^{\frac{\pi}{2}}M_{\gamma_{sr}}\left(\frac{b}{2\sin^2\theta}\right)\mathrm{d}\theta}_{K_1} - \underbrace{\frac{c}{\pi}\int_0^{\frac{\pi}{4}}M_{\gamma_{sr}}\left(\frac{b}{2\sin^2\theta}\right)\mathrm{d}\theta}_{K_2}, \quad (12)$$

where

$$K_1 = \frac{a}{\pi}\frac{\sqrt{b\overline{\gamma}_{sd}}(\mu_{SD}N_SN_D\kappa_{SD})^{\mu_{SD}N_SN_D}}{\sqrt{2\pi\mu_{SD}N_SN_D(1+\kappa_{SD})}}\left(\frac{2\mu_{SD}N_SN_D(1+\kappa_{SD})}{2\mu_{SD}N_SN_D(1+\kappa_{SD})+b\overline{\gamma}_{sd}}\right)^{\mu_{SD}N_SN_D+\frac{1}{2}}\frac{\Gamma\left(\mu_{SD}N_SN_D+\frac{1}{2}\right)\sqrt{\pi}}{\Gamma(\mu_{SD}N_SN_D+1)}\times$$

$$\sum_{J=0}^{\infty}\sum_{n=0}^{\infty}\frac{\left(\mu_{SD}N_SN_D+\frac{1}{2}\right)_{J+n}(1)_J\left(\frac{2\mu_{SD}N_SN_D(1+\kappa_{SD})}{2\mu_{SD}N_SN_D(1+\kappa_{SD})+b\overline{\gamma}_{sd}}\right)^J\left(\frac{2\mu_{SD}N_SN_D(1+\kappa_{SD})}{2\mu_{SD}N_SN_D(1+\kappa_{SD})+b\overline{\gamma}_{sd}}\right)^n}{(\mu_{SD}N_SN_D+1)_{J+n}J!n!}, \quad (13)$$

where $\mu_{SD} > 0$ is the channel fading parameter directly related to the number of clusters and κ_{SD} denotes the ratio of power in the LOS components to that of scattered components for S→D fading links. $\overline{\gamma}_{sd}$ denotes the average SNR of the source-to-destination fading link.

$$K_2 = \frac{c\sqrt{b\overline{\gamma}_{sd}}(\mu_{SD}N_SN_D\kappa_{SD})^{\mu_{SD}N_SN_D}}{2\pi\sqrt{2\mu_{SD}N_SN_D(1+\kappa_{SD})}}\left(\frac{\mu_{SD}N_SN_D(1+\kappa_{SD})}{\mu_{SD}N_SN_D(1+\kappa_{SD})+b\overline{\gamma}_{sd}}\right)^{\mu_{SD}N_SN_D+\frac{1}{2}}\frac{\Gamma\left(\mu_{SD}N_SN_D+\frac{1}{2}\right)\sqrt{\pi}}{\Gamma(\mu_{SD}N_SN_D+1)}\times$$

$$\sum_{J=0}^{\infty}\sum_{n=0}^{\infty}\sum_{p=0}^{\infty}\frac{\left(\mu_{SD}N_SN_D+\frac{1}{2}\right)_{J+N+P}(1)_m\left(\frac{1}{2}\right)_n\left(\frac{\mu_{SD}N_SN_D(1+\kappa_{SD})}{\mu_{SD}N_SN_D(1+\kappa_{SD}+b\overline{\gamma}_{sd}}\right)^J\left(\frac{2\mu_{SD}N_SN_D(1+\kappa_{SD})}{2\mu_{SD}N_SN_D(1+\kappa_{SD})+2b\overline{\gamma}_{sd}}\right)^n\left(\frac{\mu_{SD}N_SN_D(1+\kappa_{SD})}{\mu_{SD}N_SN_D(1+\kappa_{SD})+b\overline{\gamma}_{sd}}\right)^n}{\left(\frac{3}{2}\right)_{J+n+p}J!n!p!}. \quad (14)$$

Also, the SER for the R→D fading link may be expressed [40] as:

$$\overline{P_E^{R\to D}} = \underbrace{\frac{a}{\pi}\int_0^{\frac{\pi}{2}}M_{\gamma_{rd}}\left(\frac{b}{2\sin^2\theta}\right)\mathrm{d}\theta}_{\psi_1} - \underbrace{\frac{c}{\pi}\int_0^{\frac{\pi}{4}}M_{\gamma_{rd}}\left(\frac{b}{2\sin^2\theta}\right)\mathrm{d}\theta}_{\psi_2}, \quad (15)$$

where

$$\psi_1 = \frac{a}{\pi}\frac{\sqrt{b\overline{\gamma}_{rd}}(\mu_{RD}N_RN_D\kappa_{RD})^{\mu_{RD}N_RN_D}}{\sqrt{2\pi\mu_{RD}N_RN_D(1+\kappa_{RD})}}\left(\frac{2\mu_{RD}N_RN_D(1+\kappa_{RD})}{2\mu_{RD}N_RN_D(1+\kappa_{RD})+b\overline{\gamma}_{rd}}\right)^{\mu_{RD}N_RN_D+\frac{1}{2}}\frac{\Gamma\left(\mu_{RD}N_RN_D+\frac{1}{2}\right)\sqrt{\pi}}{\Gamma(\mu_{RD}N_RN_D+1)}\times$$

$$\sum_{J=0}^{\infty}\sum_{n=0}^{\infty}\frac{\left(\mu_{RD}N_RN_D+\frac{1}{2}\right)_{J+n}(1)_m\left(\frac{2\mu_{RD}N_RN_D(1+\kappa_{SD})}{2\mu_{RD}N_RN_D(1+\kappa_{RD})+b\overline{\gamma}_{rd}}\right)^J\left(\frac{2\mu_{RD}N_RN_D(1+\kappa_{RD})}{2\mu_{RD}N_RN_D(1+\kappa_{RD})+b\overline{\gamma}_{rd}}\right)^n}{(\mu_{RD}N_RN_D+1)_{J+n}J!n!}, \tag{16}$$

$$\psi_2 = \frac{c\sqrt{b\overline{\gamma}_{rd}}(\mu_{RD}N_RN_D\kappa_{RD})^{\mu_{RD}N_RN_D}}{2\pi\sqrt{2\mu_{RD}N_RN_D(1+\kappa_{RD})}}\left(\frac{\mu_{RD}N_RN_D(1+\kappa_{RD})}{\mu_{RD}N_RN_D(1+\kappa_{RD})+b\overline{\gamma}_{rd}}\right)^{\mu_{RD}N_RN_D+\frac{1}{2}}\frac{\Gamma\left(\mu_{RD}N_RN_D+\frac{1}{2}\right)\sqrt{\pi}}{\Gamma(\mu_{RD}N_RN_D+1)}\times$$

$$\sum_{J=0}^{\infty}\sum_{n=0}^{\infty}\sum_{p=0}^{\infty}\frac{\left(\mu_{RD}N_RN_D+\frac{1}{2}\right)_{J+n+p}(1)_m\left(\frac{1}{2}\right)_n\left(\frac{\mu_{RSD}N_RN_D(1+\kappa_{RD})}{\mu_{RD}N_RN_D(1+\kappa_{RD}+b\overline{\gamma}_{rd}}\right)^J\left(\frac{2\mu_{RD}N_RN_D(1+\kappa_{RD})}{2\mu_{RD}N_RN_D(1+\kappa_{RD})+2b\overline{\gamma}_{rd}}\right)^n\left(\frac{\mu_{RD}N_RN_D(1+\kappa_{RD})}{\mu_{RD}N_RN_D(1+\kappa_{RD})+b\overline{\gamma}_{rd}}\right)^n}{\left(\frac{3}{2}\right)_{J+n+p}J!n!p!}. \tag{17}$$

In the above equations $\mu_{RD} > 0$ is the channel fading parameter directly related to the number of clusters and κ_{RD} denotes the ratio of power in the LOS components to that of scattered components for R→D fading links and $\overline{\gamma}_{rd}$ denotes the average SNR of the source-to-destination fading link. The error probability of the cooperation mode, $\overline{P_E^{S\to D,R\to D}}$ may be expressed as [41], [44]:

$$\overline{P_E^{S\to D,R\to D}} = \left\{\underbrace{\frac{a}{\pi}\int_0^{\frac{\pi}{2}}M_{\gamma_{sd}}\left(\frac{b}{2\sin^2\theta}\right)\mathrm{d}\theta}_{I_1} - \underbrace{\frac{c}{\pi}\int_0^{\frac{\pi}{4}}M_{\gamma_{sd}}\left(\frac{b}{2\sin^2\theta}\right)\mathrm{d}\theta}_{I_2}\right\}\times$$

$$\left\{\underbrace{\frac{a}{\pi}\int_0^{\frac{\pi}{2}}M_{\gamma_{rd}}\left(\frac{b}{2\sin^2\theta}\right)\mathrm{d}\theta}_{\psi_1} - \underbrace{\frac{c}{\pi}\int_0^{\frac{\pi}{4}}M_{\gamma_{rd}}\left(\frac{b}{2\sin^2\theta}\right)\mathrm{d}\theta}_{\psi_2}\right\}. \tag{18}$$

$\overline{P_E^{S\to D,R\to D}}$ represents the cooperation-based signal transmission mode. If the relay decodes correctly during the relaying phase, then the destination gets the signal from the relay node and from the source node. The optimal combination is performed at the destination node using maximal ratio combining schemes. End-to-end SER of the cooperative communication fading link is:

$$\overline{P_E} = \overline{P_E^{S\to R}}\times\overline{P_E^{S\to E}} + \left(1-\overline{P_E^{S\to R}}\right)\times\overline{P_E^{S\to D,R\to D}}. \tag{19}$$

The end-to-end SER of the cooperative communication fading link may be obtained by substituting Eqs. (8), (12) and (18) into Eq. (19).

3. Simulation Results

For a MIMO-STBC S-DF relaying network, we demonstrate simulation plots of the average SER over non-homogeneous fading channel conditions. Monte Carlo simulations are conducted, and Matlab software is used for the simulations. In Figs. 1–3, for simplicity reasons, we take $\mu_{RD} = \mu_{SD} = \mu_{SR} = \mu$ and $\kappa_{RD} = \kappa_{SD} = \kappa_{SR} = \kappa$. The theoretical expressions in κ-μ fading are in the form of infinite series. However, these series converge very rapidly with an increase in the number of summation terms (N), e.g. $N = 15$ is enough to attain accuracy up to 4 decimal points. For better and assured precision, a corresponding analysis is performed with $N = 20$. In Fig. 1 we considered equal power

allocation factors with Q-PSK modulated symbols. The average end-to-end error probability versus SNR plots are shown with clear detection of κ-μ over fading channels. Average SER is plotted for $\mu = 1$, and varying κ using Eq. (16). We observe that the increment in performance is higher along with the increase in κ. In Fig. 2, SER vs. SNR is plotted for various values of κ and for a fixed value of μ. In Fig. 3, a SER vs. SNR plot is given for various values of μ and for a fixed value of κ. It has been shown that SER performance improves with the increase in the value of μ.

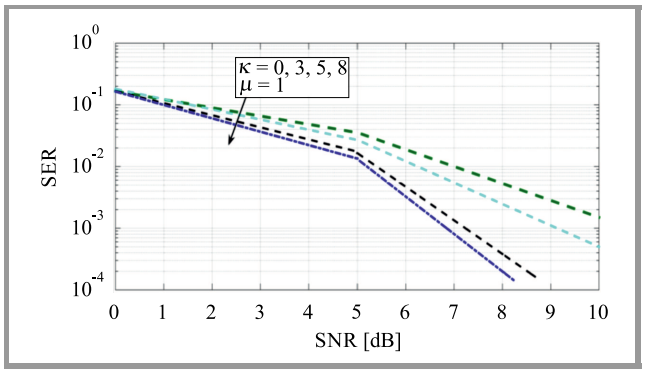

Fig. 1. Average SER performance of 4-PSK over κ-μ fading channels with different values of κ.

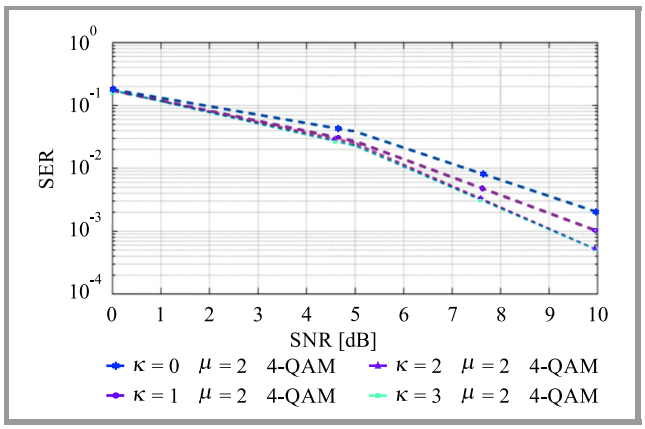

Fig. 2. Average SER performance of 4-QAM over κ-μ fading channels with different values of κ.

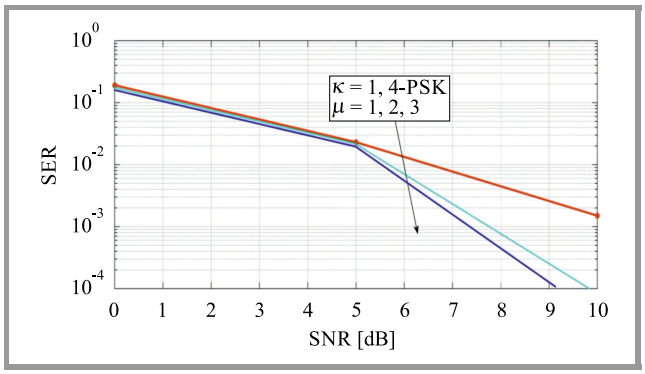

Fig. 3. Average SER performance of 4-PSK over κ-μ fading channels with different values of μ.

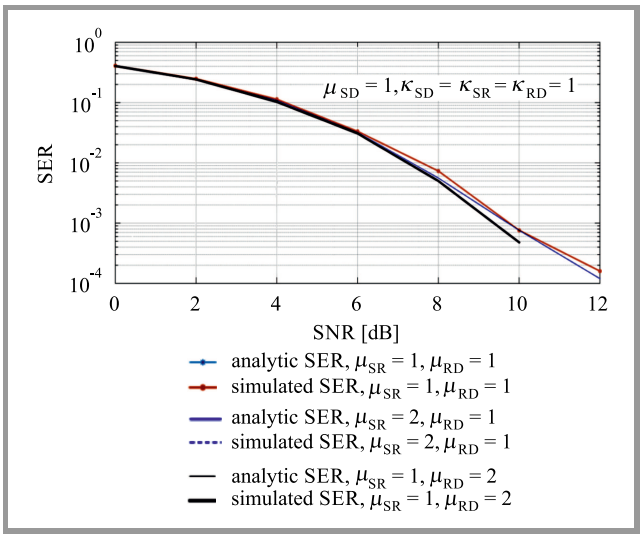

Fig. 4. SER vs. SNR plots of 4-QAM over κ-μ links.

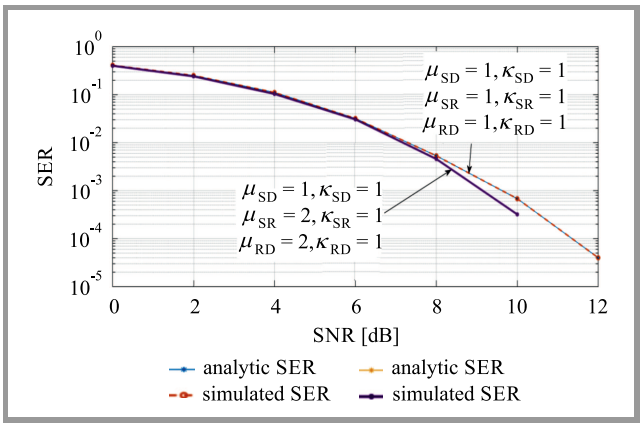

Fig. 5. SER vs. SNR plots of 4-QAM over κ-μ links for various values of κ_{ij} and μ_{ij}.

4. Conclusions

We have investigated CF expressions of the average SER for a MIMO STBC S-DF relaying network over κ-μ faded links when the input is Q-PSK and 4-QAM modulated. The average SER of QAM and QPSK are presented in the figures. Specifically, we consider the case where the S→R, R→D and S→D link is subject to the i.i.d. κ-μ fading. From the simulation results, an enhancement in SER with a stronger LOS component is observed.

Appendix A

Solution of $I_1 = \dfrac{a}{\pi}\displaystyle\int_0^{\frac{\pi}{2}} M_{\gamma_{sr}}\left(\frac{b}{2\sin^2\theta}\right)\mathrm{d}\theta$:

Let

$$t = \frac{\mu_{sr}(1+\kappa_{sr})}{\mu_{sr}(1+\kappa_{sr}) + \dfrac{b\overline{\gamma}_{sr}}{2\sin^2(\theta)}}\,. \tag{20}$$

After performing some manipulations, $\sin^2(\theta)$ is expressed as:

$$\sin^2(\theta) = \frac{b\overline{\gamma}_{sr}t}{2\mu_{sr}(1+\kappa_{sr})(1-t)} , \tag{21}$$

$$\sin(\theta) = \sqrt{\frac{b\overline{\gamma}_{sr}t}{2\mu_{sr}(1+\kappa_{sr})(1-t)}} , \tag{22}$$

$$\cos(\theta) = \sqrt{1-\frac{b\overline{\gamma}_{sr}t}{2\mu_{sr}(1+\kappa_{sr})(1-t)}} . \tag{23}$$

After differentiating Eq. (21) with respect to dt, we get:

$$2\sin(\theta)\cos(\theta)\mathrm{d}\theta = \frac{b\overline{\gamma}_{sr}\mathrm{d}t}{2\mu_{sr}(1+\kappa_{sr})(1-t)^2} . \tag{24}$$

The lower and upper limits of integral I_1 changes from 0 to 0 and from $\frac{\pi}{2}$ to $\frac{\mu_{sr}(1+\kappa_{sr})}{\mu_{sr}(1+\kappa_{sr})+\frac{b\overline{\gamma}_{sr}}{2}}$.
Substituting Eqs. (21)–(24) into integral I_1, we get:

$$I_1 = \frac{a}{\pi}\int_0^{\frac{\mu_{sr}(1+\kappa_{sr})}{\mu_{sr}(1+\kappa_{sr})+\frac{b\overline{\gamma}_{sr}}{2}}} \frac{b\overline{\gamma}_{sr}(\mu_{sr}\kappa_{sr}t)^{\mu_{sr}}\mathrm{e}^{t(1-t)^{-1}}}{2\sqrt{b\overline{\gamma}_{sr}t}\sqrt{2\mu_{sr}(1+\kappa_{sr})(1-t)-b\overline{\gamma}_{sr}t}} \tag{25}$$

For further simplification of this integral, it may be brought in the form of a confluent hypergeometric function with the substitution:

$$y = \frac{2\mu_{sr}(1+\kappa_{sr})+b\overline{\gamma}_{sr}}{2\mu_{sr}(1+\kappa_{sr})}t . \tag{26}$$

The above substitution converts the upper limit of the integral to unity without changing the lower limit of the integral. This makes it easy to represent this integral into the standard form of a confluent hypergeometric function of two variables. The confluent hypergeometric function is defined as:

$$\Phi_1(a,b,c,x,y) = \frac{\Gamma(c)}{\Gamma(a)\Gamma(c-a)} \int_0^1 t^{a-1}(1-t)^{c-a-1}(1-xt)^{-b}\mathrm{e}^{yt}\mathrm{d}t . \tag{27}$$

Further simplifications after substitution of Eq. (26) into Eq. (27) bring the integral in the form that may be given as:

$$I_1 = \frac{a}{\pi}\int_0^1 \frac{b\overline{\gamma}_{sr}y^{\mu-\frac{1}{2}}\mathrm{e}^{\frac{2\mu_{sr}(1+\kappa_{sr})}{\mu_{sr}(1+\kappa_{sr})+b\overline{\gamma}_{sr}}y}\left(1-\frac{2\mu_{sr}(1+\kappa_{sr})}{2\mu_{sr}(1+\kappa_{sr})+b\overline{\gamma}_{sr}}y\right)^{-1}}{2\sqrt{b\overline{\gamma}_{sr}}\sqrt{2\mu_{sr}(1+\kappa_{sr})(1-y)}}\times \left(\frac{2\mu_{sr}(1+\kappa_{sr})}{2\mu_{sr}(1+\kappa_{sr})+b\overline{\gamma}_{sr}}\right)\mathrm{d}y , \tag{28}$$

$$= \frac{a}{\pi}\frac{\sqrt{b\overline{\gamma}_{sr}}(\mu_{sr}\kappa_{sr})^{\mu_{sr}}}{2}\left(\frac{2\mu_{sr}(1+\kappa_{sr})}{2\mu_{sr}(1+\kappa_{sr})+b\overline{\gamma}_{sr}}\right)^{\mu_{sr}+\frac{1}{2}}\times \int_0^1 \frac{b\overline{\gamma}_{sr}y^{\mu-\frac{1}{2}}\mathrm{e}^{\frac{2\mu_{sr}(1+\kappa_{sr})}{\mu_{sr}(1+\kappa_{sr})+b\overline{\gamma}_{sr}}y}(1-y)^{-\frac{1}{2}}}{\sqrt{2\mu_{sr}(1+\kappa_{sr})(1-y)}\left(1-\frac{2\mu_{sr}(1+\kappa_{sr})}{2\mu_{sr}(1+\kappa_{sr})+b\overline{\gamma}_{sr}}y\right)}\mathrm{d}y . \tag{29}$$

The above expression may be compared with the definition of the confluent hypergeometric function given in Eq. (27) to obtain the arguments of the function as:

$$a = \mu_{sr}+\frac{1}{2} , \tag{30}$$

$$b = 1 , \tag{31}$$

$$c = \mu_{sr}+1 , \tag{32}$$

$$x = \frac{2\mu_{sr}(1+\kappa_{sr})}{2\mu_{sr}(1+\kappa_{sr})+b\overline{\gamma}_{sr}} , \tag{33}$$

$$y = \frac{2\mu_{sr}(1+\kappa_{sr})}{2\mu_{sr}(1+\kappa_{sr})+b\overline{\gamma}_{sr}} . \tag{34}$$

Thus, I_1 may be finally evaluated in the form of a confluent hypergeometric function as:

$$I_1 = \frac{a}{\pi}\frac{\sqrt{b\overline{\gamma}_{sr}}(\mu_{sr}\kappa_{sr})^{\mu_{sr}}}{2\sqrt{2\mu_{sr}(1+\kappa_{sr})}}\left(\frac{2\mu_{sr}(1+\kappa_{sr})}{2\mu_{sr}(1+\kappa_{sr})+b\overline{\gamma}_{sr}}\right)^{\mu_{sr}+\frac{1}{2}}\times \frac{\Gamma\left(\mu_{sr}+\frac{1}{2}\right)\sqrt{\pi}}{\Gamma(\mu_{sr}+1)}\Phi_1\left(\mu_{sr}+\frac{1}{2},1,\mu_{sr}+1,\frac{2\mu_{sr}(1+\kappa_{sr})}{2\mu_{sr}(1+\kappa_{sr})+b\overline{\gamma}_{sr}},\frac{2\mu_{sr}(1+\kappa_{sr})}{2\mu_{sr}(1+\kappa_{sr})+b\overline{\gamma}_{sr}}\right) . \tag{35}$$

Next, we will discuss the solution of I_2.

Appendix B

One may proceed to the solution of I_2 following the steps used for the solution of I_1 earlier. We make the same substitution as made for I_1 in Eq. (26). Thus, the same expressions will be used in the integral as discussed in Eqs. (30)–(34). However, the upper limit of the integral will now be $\frac{\mu_{sr}(1+\kappa_{sr})}{\mu_{sr}(1+\kappa_{sr})+b\overline{\gamma}_{sr}}$.
Now, it can be represented as:

$$I_2 = \frac{c}{\pi}\int_0^{\frac{\mu_{sr}(1+\kappa_{sr})}{\mu_{sr}(1+\kappa_{sr})+b\overline{\gamma}_{sr}}} \frac{b\overline{\gamma}_{sr}(\mu_{sr}\kappa_{sr}t)^{\mu_{sr}}\mathrm{e}^{t(1-t)^{-1}}}{2\sqrt{b\overline{\gamma}_{sr}t}\sqrt{2\mu_{sr}(1+\kappa_{sr})(1-t)-b\overline{\gamma}_{sr}t}}\mathrm{d}t . \tag{36}$$

For further simplification of this integral, it may be brought in the form of a confluent Lauricella's hypergeometric function of three variables with the following substitution:

$$y = \frac{\mu_{sr}(1+\kappa_{sr}) + b\overline{\gamma}_{sr}}{\mu_{sr}(1+\kappa_{sr})}\, t \ . \tag{37}$$

The above substitution converts the upper limit of the integral to unity without changing the lower limit of the integral. This makes it easy to represent this integral into the standard form of a confluent Lauricella's hypergeometric function of three variables. It is defined as:

$$\phi_1^{(3)}(a,b_1,b_2,c,x,y,z) = \frac{\Gamma(c)}{\Gamma(a)\Gamma(c-a)} \int_0^1 t^{a-1}(1-t)^{c-a-1} \times$$

$$(1-xt)^{-b_1}(1-yt)^{-b_2}\mathrm{e}^{zt}\mathrm{d}t \ . \tag{38}$$

Further simplifications after substitution of Eq. (37) into Eq. (36) bring the integral in the form that may be expressed as:

$$I_2 = \frac{c}{\pi}\frac{\sqrt{b\overline{\gamma}_{sr}}(\mu_{sr}\kappa_{sr})^{\mu_{sr}}}{2}\left(\frac{\mu_{sr}(1+\kappa_{sr})}{\mu_{sr}(1+\kappa_{sr})+b\overline{\gamma}_{sr}}\right)^{\mu_{sr}+\frac{1}{2}} \times$$

$$\int_0^1 \frac{y^{\mu_{sr}-\frac{1}{2}}\mathrm{e}^{\frac{\mu_{sr}(1+\kappa_{sr})}{\mu_{sr}(1+\kappa_{sr}+b\overline{\gamma}_{sr}}y}\left(1-\dfrac{2\mu_{sr}(1+\kappa_{sr})+b\overline{\gamma}_{sr}}{2\mu_{sr(1+\kappa_{sr})}+2b\overline{\gamma}_{sr}}y\right)^{-\frac{1}{2}}}{\sqrt{2\mu_{sr}(1+\kappa_{sr})}\left(1-\dfrac{\mu_{sr}(1+\kappa_{sr})}{\mu_{sr}(1+\kappa_{sr})+b\overline{\gamma}_{sr}}y\right)}\mathrm{d}y \ . \tag{39}$$

The above expression may be compared with the definition of the confluent Lauricella's hypergeometric function given in Eq. (38) to obtain the arguments of the function as:

$$a = \mu_{sr} + \frac{1}{2} \ , \tag{40}$$

$$b_1 = 1 \ , \tag{41}$$

$$b_2 = \frac{1}{2} \ , \tag{42}$$

$$c = \mu_{sr} + \frac{3}{2} \ , \tag{43}$$

$$x = \frac{\mu_{sr}(1+\kappa_{sr})}{\mu_{sr}(1+\kappa_{sr})+b\overline{\gamma}_{sr}} \ , \tag{44}$$

$$y = \frac{2\mu_{sr}(1+\kappa_{sr})}{2\mu_{sr}(1+\kappa_{sr})+2b\overline{\gamma}_{sr}} \ , \tag{45}$$

$$z = \frac{\mu_{sr}(1+\kappa_{sr})}{\mu_{sr}(1+\kappa_{sr})+b\overline{\gamma}_{sr}} \ . \tag{46}$$

Thus, I_2 may be finally evaluated in the form of a confluent Lauricella's hypergeometric function as:

$$I_2 = \frac{c}{\pi}\frac{\sqrt{b\overline{\gamma}_{sr}}(\mu_{sr}\kappa_{sr})^{\mu_{sr}}}{2\sqrt{2\mu_{sr}(1+\kappa_{sr})}}\left(\frac{\mu_{sr}(1+\kappa_{sr})}{\mu_{sr}(1+\kappa_{sr})+b\overline{\gamma}_{sr}}\right)^{\mu_{sr}+\frac{1}{2}} \times$$

$$\frac{\Gamma\left(\mu_{sr}+\frac{1}{2}\right)\sqrt{\pi}}{\Gamma(\mu_{sr}+1)}\, Phi_1^{(3)}\left(\mu_{sr}+\frac{1}{2},1,\frac{1}{2},\frac{3}{2},\frac{\mu_{sr}(1+\kappa_{sr})}{\mu_{sr}(1+\kappa_{sr})+b\overline{\gamma}_{sr}},\right.$$

$$\left.\frac{2\mu_{sr}(1+\kappa_{sr})}{2\mu_{sr}(1+\kappa_{sr})+b\overline{\gamma}_{sr}},\frac{\mu_{sr}(1+\kappa_{sr})}{\mu_{sr}(1+\kappa_{sr})+b\overline{\gamma}_{sr}}\right) . \tag{47}$$

Note that I_1 and I_2 have the form, respectively, of a confluent hypergeometric function and a confluent Lauricella's function. These functions are not commonly available in mathematical computation software. Thus, numerical evaluation methods for finite integrals may be used. Alternatively, these functions may be numerically evaluated using their series representation. The confluent hypergeometric function in the series form may be given as:

$$\Phi_1(a,b,c,x,y) = \sum_{J=0}^{\infty}\sum_{n=0}^{\infty}\frac{(a)_{J+n}(b)_J x^J y^n}{(c)_{J+n}J!n!} \ . \tag{48}$$

The condition for convergence of this function is $|x|<1$ which is satisfied in our case for all values of average SNR. The confluent Lauricella's hypergeometric function in the series form is:

$$\Phi_1^{(3)}(a,b,c,x,y,z) =$$

$$\sum_{J=0}^{\infty}\sum_{n=0}^{\infty}\sum_{p=0}^{\infty}\frac{(a)_{J+n+p}(b_1)_J(b_2)_n x^J y^n z^p}{(c)_{J+n+p}J!n!p!} \ . \tag{49}$$

Using Eq. (49) into Eq. (47), the integral I_2 can be expressed as in Eq. (50).

$$I_2 = \frac{c\sqrt{b\overline{\gamma}_{sr}}(\mu_{sr}N_SN_R\kappa_{sr})^{\mu_{sr}N_SN_R}}{2\pi\sqrt{2\mu_{sr}N_SN_R(1+\kappa_{sr})}}\left(\frac{\mu_{sr}N_SN_R(1+\kappa_{sr})}{\mu_{sr}N_SN_R(1+\kappa_{sr})+b\overline{\gamma}_{sr}}\right)^{\mu_{sr}N_SN_R+\frac{1}{2}}\frac{\Gamma\left(\mu_{sr}N_SN_R+\frac{1}{2}\right)\sqrt{\pi}}{\Gamma(\mu_{sr}N_SN_R+1)}\times$$

$$\sum_{J=0}^{\infty}\sum_{n=0}^{\infty}\sum_{p=0}^{\infty}\frac{\left(\mu_{sr}N_SN_R+\frac{1}{2}\right)_{J+n+p}(1)_j\left(\frac{1}{2}\right)_n\left(\frac{\mu_{sr}N_SN_R(1+\kappa_{sr})}{\mu_{sr}N_SN_R(1+\kappa_{sr}+b\overline{\gamma}_{sr}}\right)^J\left(\frac{2\mu_{sr}N_SN_R(1+\kappa_{sr})}{2\mu_{sr}N_SN_R(1+\kappa_{sr})+2b\overline{\gamma}_{sr}}\right)^n\left(\frac{\mu_{sr}N_SN_R(1+\kappa_{sr})}{\mu_{sr}N_SN_R(1+\kappa_{sr})+b\overline{\gamma}_{sr}}\right)^n}{\left(\frac{3}{2}\right)_{J+n+p}J!n!p!} \ . \tag{50}$$

References

[1] X. Xia, K. Xu, Y. Wang, and Y. Xu, "A 5G-enabling technology: benefits, feasibility, and limitations of in-band full-duplex mMIMO", *IEEE Veh. Technol. Mag.*, vol. 13, no. 3, pp. 81–90, 2018 (doi: 10.1109/MVT.2018.2792198).

[2] S. Li, L. Da, and S. Zhao, "5G Internet of Things: A survey", *J. of Indust. Inform. Integr.*, vol. 10, pp. 1–9, 2018 (doi: 10.1016/j.jii.2018.01.005).

[3] I. Parvez, A. Rahmati, I. Guvenc, A. Sarwat, and A. Dai, "A survey on low latency towards 5G: RAN, core network and caching solutions", *IEEE Commun. Surv. & Tutor.*, vol. 20, no. 4, pp. 3098–3130, 2018 (doi: 10.1109/COMST.2018.2841349).

[4] R. Shankar, V. Sachan, G. Kumar, and R. Mishra, "An investigation of two-phase multi-relay S-DF cooperative wireless network over time-variant fading channels with incorrect CSI", *Procedia Comp. Sci. J.*, vol. 125, pp. 871–879, 2018 (doi: 10.1016/j.procs.2017.12.111).

[5] V. Sachan, R. Shankar, and R. Mishra, "Selective decode-forward cooperative communication over Nakagami-m fading channel with channel estimation error", *J. of Telecommun., Electron. and Com. Engin.* (*JTEC*), vol. 9, no. 2–6, pp. 85–90, 2017 [Online]. Available: http://journal.utem.edu.my/index.php/jtec/article/download/2442/1525

[6] R. Shankar, I. Kumar, K. Pandey, and R. Mishra, "Pairwise error probability analysis and optimal power allocation for selective decode-forward protocol over Nakagami-m fading channels", in *Proc. Int. Conf. on Algor., Methodol., Models and Appl. in Emerg. Technol. ICAMMAET 2017*, Chennai, India, 2017 (doi: 10.1109/ICAMMAET.2017.8186700).

[7] Fa-Long Luo, "Full duplex device-to-device cooperative communication", U.S. Patent Application No. 15/701,007, 2019 [Online]. Available: https://patents.google.com/patent/US20190081766A1/

[8] M. Weyrich, J. Schmidt, and C. Ebert, "Machine-to-machine communication", *IEEE Software*, vol. 31, no. 4, pp. 19–23, 2014 (doi: 10.1109/MS.2014.87).

[9] A. Arash, Q. Wang and Mancuso V., "A survey on device-to-device communication in cellular networks", *IEEE Commun. Surv. & Tutor.*, vol. 16, no. 4, pp. 1801–1819, 2014 (doi: 10.1109/COMST.2014.2319555).

[10] M. Tehrani, M. Uysal, and H. Yanikomeroglu, "Device-to-device communication in 5G cellular networks: challenges, solutions, and future directions", *IEEE Commun. Mag.*, vol. 52, no. 5, pp. 86–92, 2014 (doi.10.1109/MCOM.2014.6815897).

[11] A. Amr, J. Seoane, M. Galeev, K. Komoravolu, Z. Wang, and G. Reichard, "Method and apparatus for increasing performance of communication links of cooperative communication nodes", U.S. Patent Application 10/039,061, filed July 31, 2018 [Online]. Available: https://patents.google.com/patent/US10039061B2/

[12] S. Yu, Y. Ahn, S. Choi, Y. Moon, and H. Song, "Efficient relay selection scheme utilizing superposition modulation in cooperative communication", Annals of Telecommun., vol. 1, pp. 1–6, 2019 (doi: 10.1007/s12243-019-00726-6).

[13] R. Boluda-Ruiz, A. García-Zambrana, C. Castillo-Vázquez, B. Castillo-Vázquez, and S. Hranilovic, "Amplify-and-forward strategy using MRC reception over FSO channels with pointing errors", *J. of Opt. Commun. and Network.*, vol. 10, no. 5, pp. 545–552, 2018 (doi: 10.1364/JOCN.10.000545).

[14] M. Dabiri and S. Sadough, "Performance analysis of all-optical amplify and forward relaying over log-normal FSO channels", *J. of Opt. Commun. and Network.*, vol. 10, no. 2, pp. 79–89, 2018 (doi: 10.1364/JOCN.10.000079).

[15] H. Shaoling and W. Chen, "Successive amplify-and-forward relaying with network interference cancellation", *IEEE Trans. on Wirel. Commun.*, vol. 17, no. 10, pp. 6871–6886, 2018 (doi: 10.1109/TWC.2018.2864968).

[16] L. Hongwu, Z. Ding, K. Kim, K. Kwak, and H. Poor, "Decode-and-forward relaying for cooperative NOMA systems with direct links", *IEEE Trans. on Wirel. Commun.*, vol. 17, no. 12, pp. 8077–8093, 2018 (doi: 10.1109/TWC.2018.2873999).

[17] L. Xiangli, Z. Li, and C. Wang, "Secure decode-and-forward relay SWIPT systems with power splitting schemes", *IEEE Trans. on Veh. Technol.*, vol. 67, no. 8, pp. 7341–7354, 2018 (doi: 10.1109/TVT.2018.2833446).

[18] H. Asif, R. Noor, K. Yau, I. Ahmedy, and S. Anjum, "A survey on simultaneous wireless information and power transfer with cooperative relay and future challenges", *IEEE Access*, vol. 7, pp. 19166–19198, 2019 (doi: 10.1109/ACCESS.2019.2895645).

[19] J. Ryu and J. Lee, "Trust degree-based MISO cooperative communications with two relay nodes", *Wirel. Commun. and Mob. Comput.*, vol. 2019, Article ID 7927358, pp. 1–13, 2019 (doi: 10.1155/2019/7927358).

[20] C. In, H. Kim, and W. Choi, "Achievable rate-energy region in two-way decode-and-forward energy harvesting relay systems", *IEEE Trans. on Commun.*, vol. 67, no. 7, pp. 3923–3935, 2019 (doi: 10.1109/TCOMM.2019.2901783).

[21] Y. Ye, Y. Li, L. Shi, R. Hu, and H. Zhang, "Improved hybrid relaying protocol for DF relaying in the presence of a direct link", *IEEE Wirel. Commun. Lett.*, vol. 8, no. 1, pp. 173–176, 2019 (doi: 10.1109/LWC.2018.2865476).

[22] B. Nguyen, T. Hoang, and P. Tran, "Performance analysis of full-duplex decode-and-forward relay system with energy harvesting over Nakagami-m fading channels", *AEU – Int. J. of Electron. and Commun.*, vol. 98, pp. 114–122, 2019 (doi: 10.1016/j.aeue.2018.11.002).

[23] N. T. Nguyen, M. Tran, L. T. Nguyen, D. Ha, and M. Voznak, "Performance analysis of a user selection protocol in cooperative networks with power splitting protocol-based energy harvesting over Nakagami-m/Rayleigh channels", *Electronics*, vol. 8, no. 4, pp. 448, 2019 (doi: 10.3390/electronics8040448).

[24] C. Cai, Y. Wendong, and C. Yueming, "Outage performance of OFDM-based selective decode-and forward cooperative networks over Weibull fading channels", *High Technol. Lett.*, vol. 17, no. 3, pp. 285–289, 2011 (doi: 10.3772/j.issn.1006-6748.2011.03.010).

[25] R. Shankar, K. Pandey, A. Kumari, V. Sachan, and K. R. Mishra, "C(0) protocol based cooperative wireless communication over Nakagami-m fading channels: PEP and SER analysis at optimal power", in *Proc. IEEE 7th Ann. Comput. and Commun. Worksh. and Conf. CCWC 2017*, Las Vegas, NV, USA, 2017, pp. 1–7 (doi: 10.1109/CCWC.2017.7868399).

[26] R. Shankar, I. Kumar, and K. R. Mishra, "Pairwise error probability analysis of dual hop relaying network over time selective Nakagami-m fading channel with imperfect CSI and node mobility", *Traitement du Signal*, vol. 36, no. 3, pp. 281–295, 2019 (doi: 10.18280/ts.360312).

[27] R. Shaik and K. Rama, "Performance analysis of multi-hop cooperative system under κ-μ shadowed fading channels", in *Proc. Int. Conf. on Commun. and Sig. Process. ICCSP 2019*, Chennai, India, 2019, pp. 0587–0591, 2019 (doi: 10.1109/ICCSP.2019.8698074).

[28] H. Salameh, L. Mahdawi, A. Musa, and T. Hailat, "End-to-end performance analysis with decode-and-forward relays in multihop wireless systems over α-η-μ fading channels", *IEEE Syst. J.*, vol. 1, no. 1, pp. 1–9 (doi: 10.1109/JSYST.2019.2891125).

[29] P. Kumar and K. Dhaka, "Performance analysis of a decode-and-forward relay system in κ-μ and η-μ fading channels", *IEEE Trans. on Veh. Technol.*, vol. 65, no. 4, pp. 2768–2775, 2016 (doi: 10.1109/TVT.2015.2418211).

[30] J. Zhang, X. Li, I. Ansari, Y. Liu, and K. Qaraqe, "Performance analysis of dual-hop DF satellite relaying over κ-μ shadowed fading channels", in *Proc. IEEE Wire. Commun. and Network. Conf. WCNC 2017*, San Francisco, CA, USA, 2017, pp. 1–6 (doi: 10.1109/WCNC.2017.7925541).

[31] A. Kodide, "Performance analysis of a cooperative communication network over κ-μ shadowed fading for different relaying protocols", Master Thesis, Faculty of Engineering, Department of Applied Signal Processing, Blekinge Institute of Technology, Karlskrona, Sweden, 2015 [Online]. Available: https://pdfs.semanticscholar.org/5ce4/eb4ab03b63b69af858d1f9375d9b7291284d.pdf"

[32] L. S. Cotton, "Human body shadowing in cellular device-to-device communications: channel modeling using the shadowed κ-μ fading model", *IEEE J. on Selec. Areas in Commun.*, vol. 33, no. 1, pp. 111–119, 2015 (doi: 10.1109/JSAC.2014.2369613).

[33] W. Cheng, H. Hung, and H. Lu,"A novel two-stage fusion detector based on maximum ratio combining and max-log rules", in *Proc. of the 2nd High Perform. Comp. and Cluster Technol. Conf. HPCCT 2018*, Beijing, China, 2018, pp. 116–120 (doi: 10.1145/3234664.3234673).

[34] R. Shankar and K. R. Mishra, "Outage probability analysis of selective-decode and forward cooperative wireless network over time varying fading channels with node mobility and imperfect CSI condition", in *Proc. TENCON 2018 – 2018 IEEE Region 10 Conf.*, Jeju, South Korea, 2018, pp. 0508–0513 (doi: 10.1109/TENCON.2018.8650275).

[35] V. Sachan, I. Kumar, R. Shankar, and R. Mishra, "Analysis of transmit antenna selection based selective decode forward cooperative communication protocol", *Traitement du Signal*, vol. 35, no. 1, pp. 47–60, 2018 (doi: 10.3166/ts.35.47-60).

[36] M. D. Yacoub, "The κ-μ distribution: A general fading distribution", in *Proc. IEEE 54th Veh. Technol. Conf. VTC Fall 2001, Atlantic City*, NJ, USA, 2001, vol. 3, no. 1, pp. 1427–1431 (doi: 10.1109/VTC.2001.956432).

[37] M. D. Yacoub, "The α-μ distribution: A general fading distribution", in *Proc. 13th IEEE Int. Symp. on Pers., Indoor and Mob. Radio Commun.*, Pavilhao Altantico, Lisbon, Portugal, 2002, vol. 2, pp. 629–633 (doi: 10.1109/PIMRC.2002.1047298).

[38] M. D. Yacoub, "The α-μ distribution: A physical fading model for the Stacy distribution", *IEEE Trans. on Veh. Technol.*, vol. 56, pp. 27–34, 2007 (doi: 10.1109/TVT.2006.883753).

[39] M. D. Yacoub, "The κ-μ distribution and the η-μ distribution", *IEEE Antenn. and Propag. Mag.*, vol. 49, pp. 68–81, 2007 (doi: 10.1109/MAP.2007.370983).

[40] M. K. Simon and M.-S. Alouini, *Digital Communication Over Fading Channels: A Unified Approach to Performance Analysis*. Wiley, (ISBN: 9780471317791).

[41] K. J. R. Liu, A. K. Sadek, W. Su, and A. Kwasinski, *Cooperative Communications and Networking*. Cambridge University Press, 2008 (ISBN: 9780511754524, doi: 10.1017/CBO9780511754524).

[42] I. S. Gradshteyn and I. M. Ryzhik, *Table of Integrals, Series, and Products*, 8th ed. Academic Press, 2014 (ISBN 978-0-12-384933-5, doi: 10.1016/C2010-0-64839-5).

[43] I. S. Gradshteyn and I. M. Ryzhik, *Table of Integrals, Series, and Products*, 7th ed. Academic Press, 2007 (ISBN: 9780123736376).

[44] R. Shankar, I. Kumar, and K. R. Mishra, "Pairwise error probability analysis of dual hop relaying network over time selective Nakagami-m fading channel with imperfect CSI and node mobility", *Traitement du Signal*, vol. 36, no. 3, pp. 281–295, 2019 (doi: 10.18280/ts.360312).

[45] H. M. Srivastava, A. Çetinkaya, and I. Onur Kiymaz, "A certain generalized Pochhammer symbol and its applications to hypergeometric functions", *Appl. Mathem. and Comput.*, vol. 226, pp. 484–491, 2014 (doi: 10.1016/j.amc.2013.10.032).

Ravi Shankar received his B.E. degree in Electronics and Communication Engineering from Jiwaji University, Gwalior, India, in 2006. He received his M.Tech. degree in Electronics and Communication Engineering from GGSIPU, New Delhi, India, in 2012. He received a Ph.D. in Wireless Communication from the National Institute of Technology Patna, Patna, India, in 2019. He was an Assistant Professor at MRCE Faridabad, from 2013 to 2014, where he was engaged in researching wireless communication networks. He is presently an Assistant Professor at MITS Madanapalle, Madanapalle, India. His current research interests cover cooperative communication, D2D communication, IoT/M2M networks and network protocols. He is a student member of IEEE.

E-mail: ravishankar@mits.ac.in
ECE Department
MITS Madanapalle
Madanapalle-517325, AP, India

Lokesh Bhardwaj received his B.Tech. degree in Electronics and Communication Engineering from Maharishi Dayanand University, Rohtak, in 2007 and M.Tech. in Electronics and Communication Engineering from Thapar University, Patiala, in 2010. He is currently working as an Assistant Professor with the Department of Electronics and Communication Engineering, Manav Rachna University, Faridabad. His research interests focus on wireless communications. He is currently pursuing a Ph.D. from the National Institute of Technology, Patna. His current research interests include Massive MIMO, D2D Communication, M2M networks and network protocols. He is a student member of IEEE.

E-mail: lokesh@mru.edu.in
ECE Department
National Institute of Technology Patna
Patna-800005, India

Ritesh Kumar Mishra received his B.E. degree in Electronics and Communication Engineering from Shivaji University, Kolhapur, India, in 1998. He received his M.Tech. degree in Electronics and Communication Engineering from University of Burdwan, WB, India, in 2004. He received his Ph.D. in Wireless Communication from LNMU, Bihar, India, in 2011. He is presently working as an Assistant Professor at the National Institute of Technology Patna, Patna, India and has been engaged in researching wireless communication networks. His current research interests focus on cooperative communication, D2D communication, IoT/M2M networks, and network. He is a member of IEEE, the Institution of Engineers and the Indian Society of Technical Education.

E-mail: ritesh@nitp.ac.in
ECE Department
National Institute of Technology
Patna Patna-800005, India